Energy & Environmental Science

Accepted Manuscript

ROYAL SOCIETY OF CHEMISTRY

www.rsc.org/ees

Cite this: DOI: 10.1039/c0xx00000x

www.rsc.org/xxxxxx

ARTICLE TYPE

A survey of diverse earth abundant oxygen evolution electrocatalysts showing enhanced activity from Ni-Fe oxides containing a third metal

James B. Gerken, Sarah E. Shaner, Robert C. Massé, Nicholas J. Porubsky, and Shannon S. Stahl*

Received (in XXX, XXX) Xth XXXXXXXXX 20XX, Accepted Xth XXXXXXXXX 20XX

DOI: 10.1039/b000000x

Mixed metal oxides comprise a diverse class of materials that are appealing as potential water oxidation electrocatalysts. Here we report combinatorial screening of nearly 3500 trimetallic $A_xB_yC_zO_q$ mixed metal oxide compositions that led to the discovery of electrocatalysts with enhanced activity relative to, *inter alia*, the well-studied pure oxides, ABO_3, and AB_2O_4 stoichiometries of those metals. Using a fluorescence-based parallel screening method, we directly detect electrolytic oxygen-evolution activity of catalyst arrays under alkaline conditions. From these data, composition-activity relationships amongst mixed oxides composed of earth-abundant elements have been determined. Significant sustained activity is observed only in the presence of Co or Ni, and the data draw attention to synergistic interactions between these redox-active ions and Lewis-acidic cations, such as Fe, Al, Ga, and Cr. The best activities are observed with oxides composed of Ni and Fe, together with another element.

Introduction

Electrocatalytic water oxidation is a key component of most photoelectrochemical strategies for conversion of solar energy into chemical fuels (Scheme 1).[1] Metal oxides are the most promising electrocatalysts for this transformation,[2,3,4] and are already used in commercial electrolyzers. For example, alkaline electrolyzers employ nickel oxide coated anodes.[5] While a great body of literature exists concerning the activity and stability of oxygen evolution reaction (OER) electrocatalysts composed of earth abundant materials, the state of the field still precludes rational design of an optimal mixed oxide catalyst. Such catalysts have shown enhanced activity compared to single-metal oxide compositions, with ferrite, spinel, and perovskite stoichiometries being extensively studied.[1a,6,7] There have been some studies of non-stoichiometric mixed oxides as well, albeit with limited coverage of compositional diversity space.[8] The number of combinations of earth abundant cations in more complex oxide mixtures far exceeds the number heretofore reported or that are practical to synthesize sequentially and test by traditional methods. In this context, combinatorial methods provide an appealing approach to identify promising catalyst compositions.

An effective catalyst active site is likely to contain multiple redox-active metal ions capable of buffering the multi-electron processes necessary for water oxidation. Selection of mid-to-late first-row transition metals provides the capacity for multiple

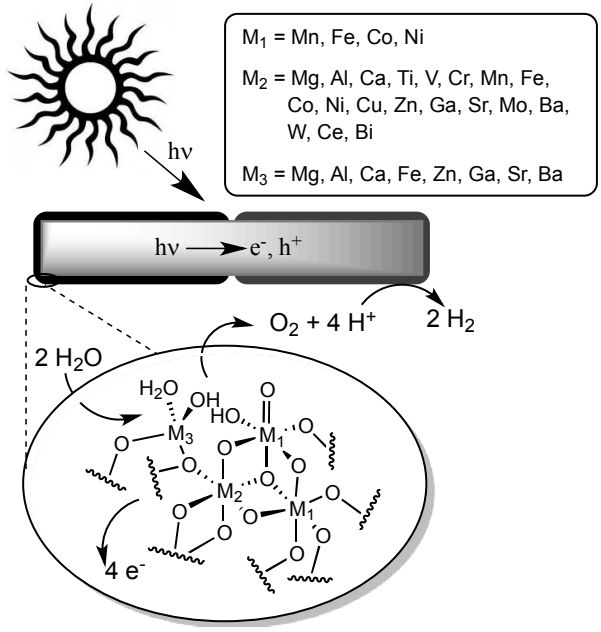

Scheme 1 Approach to photoelectrochemical energy storage consisting of a semiconductor photoelectrode coupled to catalysts for O_2 evolution and H_2 production. Metals within the oxide electrocatalyst can have different roles, e.g., M_1 - multi-electron redox, M_2 - μ-oxo ligand modulation, M_3 - Lewis-acid modulation of water nucleophilicity and proton-transfer.

Broader Context

Effective water oxidation electrocatalysts are necessary within many schemes to store renewable energy, such as sunlight, as chemical fuels. The oxidation of water to molecular oxygen is a challenging reaction because it involves the transfer of four protons and four electrons with the formation of an oxygen-oxygen bond. To be technologically relevant, the reaction requires catalysis, and the catalysts must withstand strongly oxidizing conditions and, ideally, will be composed of earth-abundant elements. Base-metal oxides in alkaline conditions have emerged as a promising class of materials. The OER activity of known monometallic oxide catalysts, such as nickel and cobalt oxides, can be further improved through the incorporation of other metal ions. However, it is difficult to predict which formulations will produce the best catalysts. For this reason, we have applied a parallel screening assay to screen diverse mixed-metal oxides containing between one and three metals for OER activity. Using this assay, several new compositions including oxides composed of Ni and Fe and a third element have been identified as particularly active electrocatalysts.

oxidation states at relevant potentials using earth abundant elements. These redox-active ions are bound to each other with bridging oxo or hydroxo linkages and are similarly linked to the electrode surface. Substituting different Lewis acids (M_2, M_3 in Scheme 1) into the oxide modulates the ligand field properties of these peripheral (hydr)oxo groups.[9] Main group, rare-earth, and early transition metals can act as Lewis acids with diverse charges, radii, and hardnesses.[10] These considerations find biological precedent in the oxo-bridged Mn_4Ca core of the photosystem II oxygen-evolving center,[11] wherein the importance of redox-inert cations in controlling the reduction potentials of Mn-based catalytic intermediates has been demonstrated.[12]

In order to implement these concepts, we recently developed a fluorescence-based combinatorial assay to detect oxygen evolution activity across arrays of potential metal oxide catalysts.[13] This method complements earlier parallel combinatorial approaches to identify photoanode[14] and electrocatalyst[15] materials for water oxidation, as well as sequential methods, such as scanning electrochemical microscopy and other robotic methods,[16] to identify (photo)electrocatalysts for water oxidation. In our initial report, we described preliminary screening of 400+ metal oxide combinations. This work identified lead compositions that resulted in the characterization of a well defined inverse spinel oxide, $NiFeAlO_4$, that exhibits higher activity than known Ni- and NiFe-based oxide electrocatalysts.[17]

Here we report a variant of our combinatorial assay that enables an order-of-magnitude improvement in throughput, together with the results of screening potential catalysts containing up to three different metals. The compositional diversity space covered in this investigation is the broadest reported to date, and the results amplify the insights gained in our preliminary study. Catalytically active cobalt and nickel oxides benefit significantly from the presence of metal ions that show little or no independent water oxidation activity, and the compositions showing the highest activity contain mixtures of Ni, Fe and a third metal. Overall, this assay demonstrates an efficient semi-quantitative means of identifying promising compositions that warrant more-systematic investigation.

Results

Apparatus

The screening assay apparatus (Figures 1, S2†) consists of a sealed polycarbonate compartment containing an anode with a 15 × 14 rectangular array of varied oxide compositions, electrolyte solution, and a Ni wire counter electrode. The array of 210 positions on the electrode are arranged to ensure spatial resolution of oxygen evolved from different catalysts. The apparatus is interfaced with an optical system for detecting oxygen evolution (see ESI† for details). A stainless steel mesh, coated with a dual-chromophore fluorescent oxygen-sensitive paint,[18] is positioned parallel to the anode at a distance of approx. 2 mm. During electrolysis, the mesh is illuminated with ca. 400 nm light pulses from a defocused diode laser array synchronized to a digital camera. This mesh fluoresces red and green in the absence of oxygen, but only green in the presence of oxygen, and the emitted light is detected by the camera. Electrolysis under

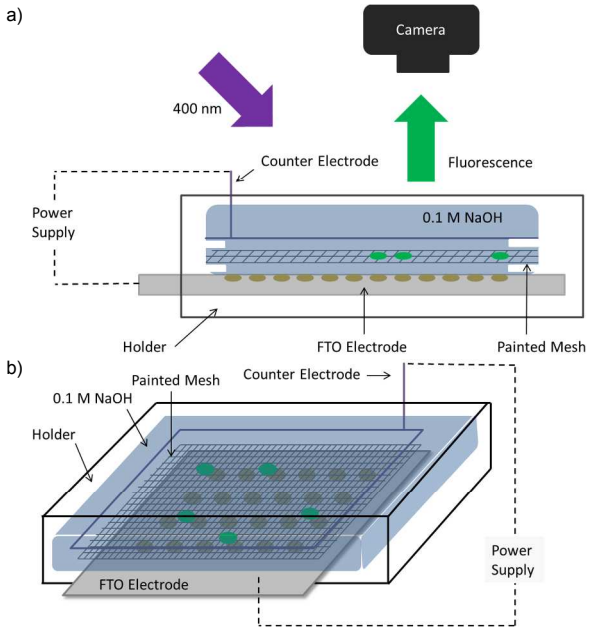

Figure 1 Schematic drawings of the a) side and b) perspective views of the screening apparatus.

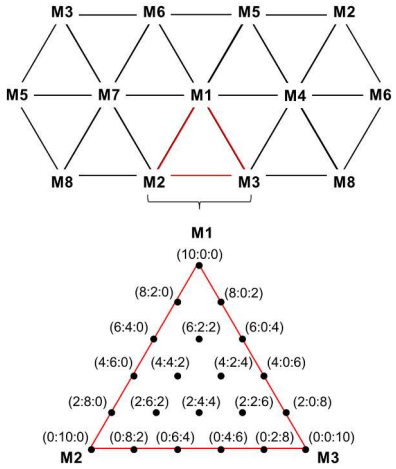

Figure 2 Mixed metal oxide diversity space encompassed on a single catalyst array. Fourteen triads of eight metals, where each triad consists of trimetallic mixtures $A_{(100\,\%\,-\,p)}B_{(p\,-\,q)}C_qO_m$, where p and q are varied in steps of 20 % from 0 to 100 % and m freely varies to fit the oxidation states of the cations, can be accommodated on one electrode.

constant-current conditions (5 mA) were selected for screening (Figures S1, S2†). To assess the sensitivity of the results to the electrolysis method, experiments were replicated under constant-potential conditions (670 mV vs. Ag/AgCl), as well as at a constant current of 10 mA (Figures S3, S4†). No significant differences were observed in the relative activities, although some loss of resolution was observed at higher currents (10 mA) due to the increased amount of O_2 produced.

Catalyst Arrays

To make a tractable selection of the mixed oxide diversity space, we elected to study trimetallic mixtures $A_{(100\,\%\,-\,p)}B_{(p\,-\,q)}C_qO_m$, where p and q were varied in steps of 20 % from 0 to 100 % and m freely varies to fit the oxidation states of the cations in the catalyst resting state. A single electrode array is optimally filled

by fourteen triads of eight metals. Our previous study identified $Co_{40}Fe_{40}Ni_{20}$ oxide as a reliable reference, and several spots were included in the array for calibration purposes. The different compositions fit within the 210 available positions by removal of duplicates among the triads (Figures 2 and S6†).

Arrays were prepared on fluorine-doped tin oxide (FTO)-coated glass by mixing and depositing aliquots of precursor solutions of the corresponding metal salts using a liquid-handling robot. Each FTO electrode was then calcined in air at 500 °C for 6 h to form the mixed oxides. Following calcination, the array was electrolyzed at 5 mA for 60 minutes to bring the oxides to steady-state catalytic conditions.

The triads of metals selected for screening were based on the considerations outlined in the Introduction, and they consisted of a diverse mix of earth-abundant redox-active and Lewis acidic metals: Mg, Al, Ca, Ti – Ga (inclusive), Sr, Mo, Ba, Ce, W, and Bi. Screens were performed on 459 unique triads distributed on 71 electrodes for a total of 12134 combinations, including 3451 unique compositions. The deposition protocol dictated that many triads were replicated on multiple electrodes, and the catalytic activities presented below were averaged in these cases.

Catalytic Activity Measurement and Data Processing

The catalyst arrays were electrolyzed at 5 mA in the sealed apparatus filled with argon-purged 0.1 M NaOH. Evolution of oxygen from the electrode was monitored by taking sequential photographs of the fluorescent mesh during the electrolysis (*cf.* Figure 1a). Oxygen-dependent quenching of the red fluorescence signal was evident as green spots in the photographs. Data obtained from a representative electrode containing oxides composed of Ca, Ti, Cr, Co, Ni, Ga, W, and/or Bi are depicted in Figure 3. The sequential images of the mesh were processed as described previously[13] and elaborated in the ESI† to determine the magnitude of the red fluorescence quenching over individual spots in the array.[19] Greyscale images produced in this manner have intensities proportional to the relative activities of the catalysts in the array. False-colour mapping of the greyscale images enables straightforward visualization of the data (Figure 3b).[20] The activity of each catalyst was normalized relative to the activity of nickel oxide, which was assigned an activity of 1.0, and plotted on ternary composition diagrams for each triad in the array (Figure 3c). All of the screening data were acquired and analyzed using this protocol, and the full set of raw data are tabulated in the ESI†. The relative O_2 evolution rates of different catalyst compositions were reproducible across multiple runs with the same electrode. Identical catalyst compositions that appeared on different electrodes also showed good reproducibilities, and average activities are reported in these instances.

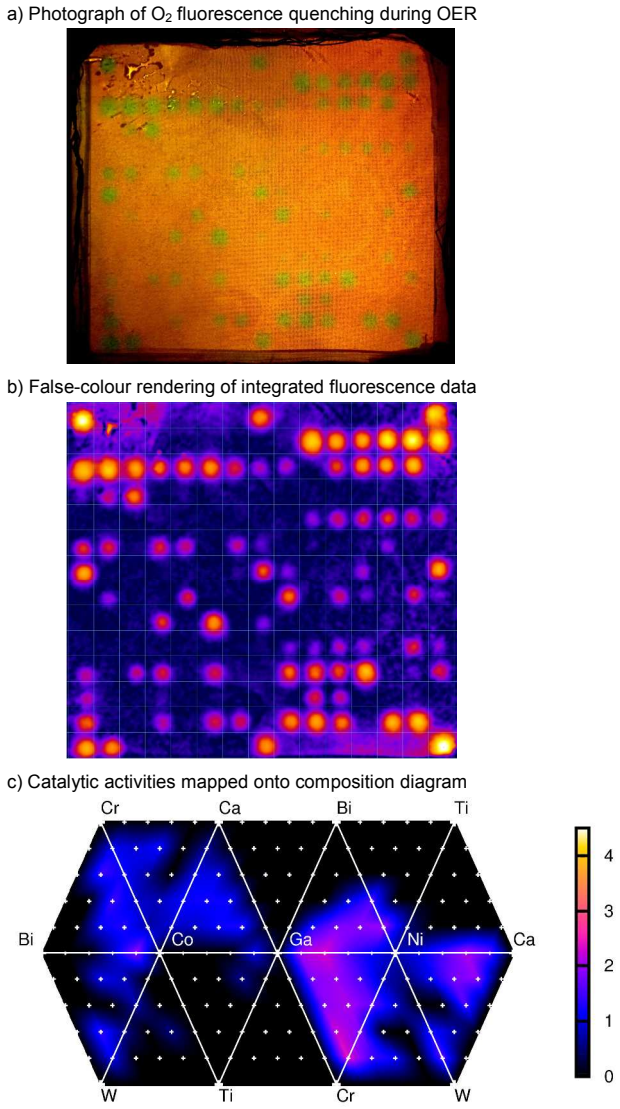

Figure 3 a) Representative photograph of the fluorescence quenching indicative of O_2 production after 6 min. of electrolysis (contrast-enhanced for print). b) False-colour rendering of the fluorescence data integrated over the electrolysis time. c) Activities, relative to nickel oxide, of the catalyst compositions on the electrode in (b) mapped back onto the composition diagrams.

Correlation of the observed catalytic activities with the elemental composition of the catalysts shows that high-activity

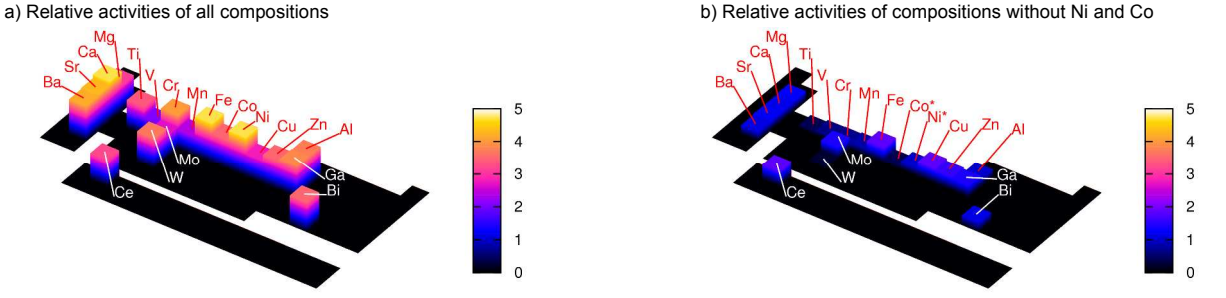

Figure 4 Activity of the most active composition containing each element: a) all-inclusive, b) compositions without Co or Ni (Co* and Ni* activities are for the monometallic oxides).

catalysts predominantly contain Co or Ni (Figure 4). Whereas considerable effort has focused on the electrocatalytic activity of Mn-based oxides,[4c,8f,g,11d,12b,21] compositions containing Mn showed relative inactivity in this study compared to those containing Co and Ni. A broad collection of relative activity data for Co- and Ni-containing oxides is compiled in Table 1 and highlights the beneficial effect of synergistic metal ions within these oxides.

Tafel Measurements

The high-activity catalyst compositions identified in this study were analyzed further by performing steady-state Tafel analysis on independently prepared electrodes. Some less active compositions, which included Ni, Co, and Ni-Fe binary oxides, were also tested. The currents obtained from the Tafel analysis were normalized to the oxide geometric area on the FTO electrode (Figures 5, S7†) or the electrochemical surface area (Figure S8†). The trimetallic oxides evaluated by Tafel analysis outperform the corresponding nickel and cobalt single-metal oxides, as predicted by the screening data. The highest activities were observed with oxides composed of Ni-Fe-Ga, Ni-Fe-Cr, Ni-Fe-Mo, Ni-Fe-Ca, and Ni-Fe-Al. Tafel slopes obtained from these materials range from 30 – 38 mV/dec (see Table S1†).

Nearly all of the Tafel activity data show good correlation with the data obtained from the combinatorial assay (Figure 6). The exceptions are Ni-Fe-Sr and Ni-Fe-Ca 40:20:40 oxide materials, which showed substantially better activity in the combinatorial screen relative to the Tafel activity. We suspect that these outliers may reflect Sr^{2+} or Ca^{2+} leaching under the higher potentials and at the longer times required for the Tafel experiments (see below). Overall, the Tafel studies validate that the fluorescence-based assay is a robust parallel screening method to assess oxygen-evolution activity from a diverse set of possible catalyst compositions distributed on an electrode. The best catalysts identified from the Tafel experiment again highlight catalysts composed of Ni and Fe, together with another element.

Discussion

The present investigation has enabled a systematic assessment of diverse mixed metal oxide electrocatalysts that have been prepared and tested under uniform conditions. This broad survey featured oxide materials composed of up to three different metal ions from among a collection of 19 earth abundant elements. Of

Table 1 Maximal average activity of cobalt- and nickel-containing triads and dyads. Relative activities > 1 in yellow, > 3 in orange, and > 4 in red.

	Cobalt-Based Oxides																	0.4
	0.6[a]	0.8	1.0	0.4	0.6	1.0	0.6	0.8	1.6	0.6	0.6	0.6	1.0	0.6	1.0	0.8	0.8	1.2	Co
	Mg	Al	Ca	Ti	V	Cr	Mn	Fe	Ni	Cu	Zn	Ga	Sr	Mo	Ba	Ce	W	Bi	
Mg		0.2[b]	0	0	0.2	0.8	0.4	2.0	2.0	0.2	0.4	0	0	0	0.8	1.4	0.8	1.0	Mg
Al			1.2	0	0.4	0.2	0.6	0.6	2.6	0.4	0.4	0.6	1.0	0.8	1.6	1.8	0.8	3.4	Al
Ca	1.2[d]			0.2	1.0	1.0	0.4	1.6	3.2	0.6	2.4	1.4	1.4	0.6	0.8	1.8	1.8	2.8	Ca
Ti	2.4	3.4			0	0	0	0	0	0	0	0.6	0	1.2	0	0	1.2	0	Ti
V	0	0.8	0			0.6	0	1.6	1.2	0.8	0.6	0.8	1.2	0	0.4	0.4	1.0	0.6	V
Cr	0.8	1.2	1.0	0.8			0.2	2.0	2.4	1.4	0.6	0.6	1.4	0	2.2	0	2.8	1.2	Cr
Mn	2.4	3.2	3	3.4	2.0			2.0	1.6	0	0.2	0	1.0	0.4	0	0	0.8	0.6	Mn
Fe	0	2.0	0.8	0.6	1.6	1.0			2.4	0.4	1.2	0.8	2.6	2	3	2.6	1.8	0.6	Fe
Co	3.2	3.8	4.8	0.6	2.0	4.0	2.4			0.2	3.4	2.2	3.4	1.4	3.2	1.6	1.8	1.4	Ni
Cu	2.0	2.6	3.2	0	1.2	2.4	1.6	2.4			0.8	1.4	0.4	0.4	0.8	0.2	1.4	0.8	Cu
Zn	0.2	1.8	0.4	0	0	1.0	0	0	0.2			0.4	0.8	0.8	2.0	0.4	0	1.8	Zn
Ga	1.4	2.8	3.0	0	1.0	3.4	0.2	1.8	3.4	1.0			1.6	0.8	2.8	1.4	2.4	2.4	Ga
Sr	2.2	2.0	2.8	2.6	1.6	2.4	1.4	3.8	2.2	1.4	1.0			1.0	2	1.2	1.4	1.6	Sr
Mo	1.4	3.0	3.4	0.6	1.4	1.8	0.8	4.4	3.4	0.4	1.2	2.4			1.0	0.4	0	0.6	Mo
Ba	1.0	1.4	2.4	1.6	1.2	1.2	1.6	2.4	1.4	0	2.0	2.2	1.8			1.2	1.4	0.6	Ba
Ce	2.0	2.6	3.6	1.8	1.0	2.6	1.0	4.2	3.2	0.4	1.8	2.4	2.4	1.2			1.2	0	Ce
W	1.0	2.2	1.8	0.8	1.6	2.2	1.0	3.2	1.6	0	0	3.0	0.6	0.8	1.2			1.2[d]	W
Bi	1.4	1.8	1.0	1.2	1.4	1.8	1.4	3.6	1.8	2.8	1.2	2.4	1.6	2.6	1.4	1.6			Bi
	Mg	Al	Ca	Ti	V	Cr	Mn	Fe	Co	Cu	Zn	Ga	Sr	Mo	Ba	Ce	W	Bi	
	1.2[c]	2.4	2.0	1.0	1.0	2.4	1.0	2.4	1.6	1.0	1.4	1.8	1.8	1.6	1.8	1.6	1.0	1.0	
Ni 1.0	Nickel-Based Oxides																		

[a] This row ranked according to the highest of each Co-M dyad (e.g., the maximum of the $Co_{20}Mg_{80}O_x$, $Co_{40}Mg_{60}O_x$, $Co_{60}Mg_{40}O_x$, $Co_{80}Mg_{20}O_x$ mixtures). [b] Highest activity in the interior (trimetallic oxides only) of each Co-containing triad (e.g., the maximum of the $Co_xMg_yAl_zO_q$ mixtures). [c] This row ranked according to the highest of each Ni-M dyad (e.g., the maximum of the $Ni_{20}Mg_{80}O_x$, $Ni_{40}Mg_{60}O_x$, $Ni_{60}Mg_{40}O_x$, $Ni_{80}Mg_{20}O_x$ mixtures). [d] Highest activity in the interior (trimetallic oxides only) of each Ni-containing triad (e.g., this cell is the maximum of the $Ni_xMg_yAl_zO_q$ mixtures).

the nearly 3500 oxides tested, less than 1/3 of the compositions tested showed significant activity (≥ 0.4 relative to nickel oxide). High OER activity was only observed with compositions containing cobalt or nickel. Over half of the compositions surveyed did not contain cobalt or nickel, and none of these showed activity twice that of nickel oxide. Numerous trimetallic oxides show enhanced activity over analogous bimetallic oxide compositions. For every bimetallic mixture tested that contained either cobalt or nickel, there exists a third metal capable of producing increased performance upon its admixture (cf. Table 1).

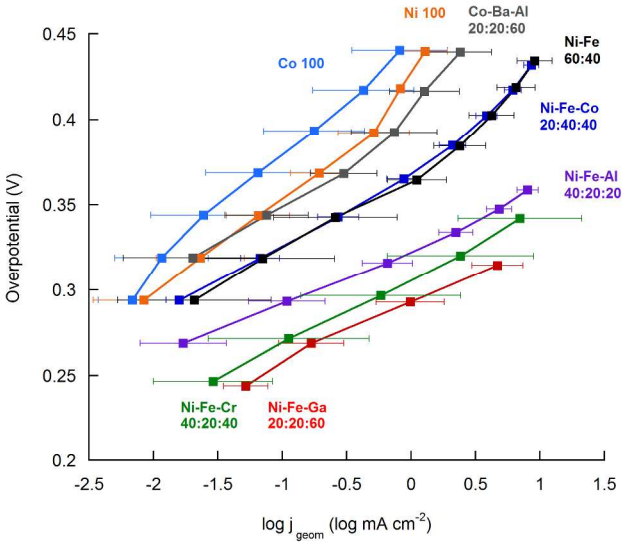

Figure 5 Tafel data for selected catalyst compositions from the combinatorial screening assay. X-axis error bars indicate one standard deviation based on multiple samples. Current densities are based on the geometric surface areas of the of the catalyst films.

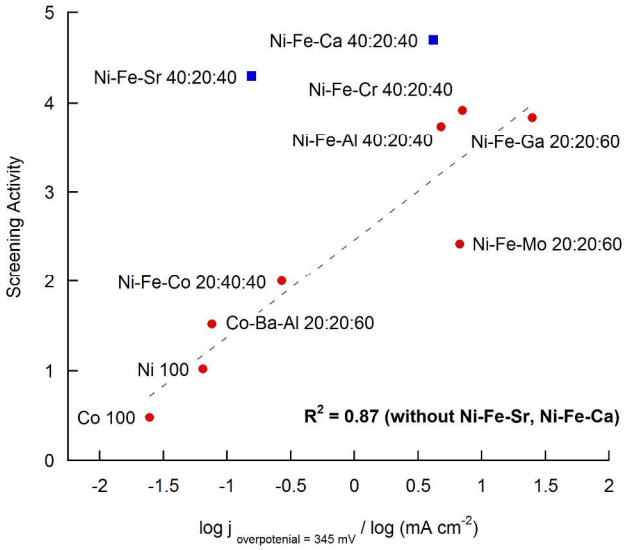

Figure 6 Correlation between catalyst activity derived from the fluorescence-quenching assay (activity reported relative to NiO; cf. Table 1) and steady-state Tafel activity at η = 345 mV.

Examination of the relative activities in Figure 4 and Table 1 show that Ni-based oxides are significantly more active than Co-based oxides. Bimetallic Ni-Fe oxides have attracted considerable attention as water oxidation catalysts,[2c,8a-e,22] and nickel oxides incorporating 10 – 40% Fe have been reported to be particularly promising compositions. These results are consistent with the identification of Ni-Fe 80:20 and 60:40 as the most active NiFe binary oxides in our screening (see ESI†). We note that there are several iron-free Ni oxide compositions (Table 1) that outperform the best Ni-Fe binary mixture, but the most active compositions overall contain Ni, Fe and a third metal. There have also been some focused investigations of trimetallic and more complex NiFe oxide mixtures, such Ni-Fe-Co[8f,i,16d,e] and Ni-Fe-Mo.[8h] The results reported here show good agreement with the previously reported activity-composition trends within these triads. The present work, together with our earlier study,[13] however, show that Ni-Fe-M oxides constitute a broad family of highly promising electrocatalyst compositions for water oxidation. The aggregate results highlight the synergistic effect of adding a third metal ion to Ni-Fe oxides.

Not all variations in activity are likely to be due to effects from changes in the composition of the catalyst itself. Some of the high-activity compositions summarized in Table 1 contain alkaline-earth metals. It is plausible that these data reflect increased surface area following leaching of the alkaline-earth ions, which can be highly soluble under the electrolysis conditions. For example, the recently observed high apparent activities of Ba- and Sr-containing perovskite catalysts[7b] have been subsequently attributed to A-site leaching of Sr and Ba with concomitant catalyst activation due to the resulting increase in solvent-accessible B-site cations.[7c] Our data suggest that Ca is susceptible to similar leaching (cf. Figure 6).

The screening data also highlight that nominally similar ions (same charge, comparable size, similar point-of-zero-charge for the oxide[23]), such as Fe^{3+} and Ga^{3+}, were not necessarily interchangeable with respect to catalytic activity. For example, with Ni-based oxides containing admixtures of Al, Fe, and/or Ga, gallium was found to be a poor substitute for iron (Figure 7). On the other hand, Ga can take the place of Al with little loss of activity. Fe^{III} and Ga^{III} might be expected to have similar effects on the basis of their similar charge and M-O bond distance, and gallium is often used as an analogue of iron(III).[24]

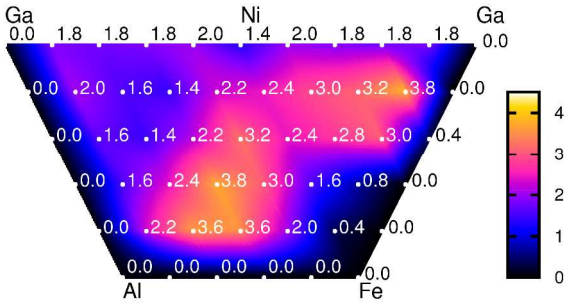

Figure 7 Activity vs. composition plot for three triads containing Ni, in combination with Al, Fe, and/or Ga. $Al_{40}Fe_{20}Ni_{40}$ and $Fe_{20}Ni_{20}Ga_{60}$ were found to have the highest levels of activity in this region of composition space.

In contrast to the beneficial effect of chromium or iron on mixed oxide catalysts, manganese admixtures show a decreased activity relative to pure cobalt or nickel oxide. The relative inactivity of manganese-containing oxides is noteworthy given

this element's central role in biological oxygen evolution. However, activities of different polymorphs of manganese oxides have been reported to vary markedly, and this feature may account for the poor Mn activities observed here.[7d,21]

Conclusions

In this study, we have used a parallel-screening assay to probe the composition-activity relationship among a diverse set of nearly 3500 earth abundant mixed oxide catalysts for electrochemical water oxidation. Several valuable trends and promising compositions have been identified. Cobalt or nickel was found to be essential for low-overpotential water oxidation catalysis under the alkaline conditions studied here, and the activity of these single-metal oxides can be enhanced by the incorporation of additional metal ions into the oxide. In particular, NiFe oxides containing a third metal (e.g., Ni-Fe-Al, Ni-Fe-Ga, and Ni-Fe-Cr) emerged as highly effective catalysts. These observation warrant further invesigation to probe the mechanistic basis for the influence of the third metal.[25]

Acknowledgements

The authors acknowledge funding support by the NSF CCI grant CHE-0802907. R. C. M. acknowledges support from a Holstrom Environmental Scholarship. Gifts of materials by Prof. Eric Strieter and the late Prof. Howard Zimmerman were helpful in producing the experimental apparatus. The authors thank Profs. Bruce Parkinson (Univ. Wyoming), Jennifer Schuttlefield (Univ. Wisconsin-Oshkosh), and Allen J. Bard (Univ. Texas-Austin) for illuminating discussions.

Notes and references

Department of Chemistry, University of Wisconsin-Madison, 1101 University Ave, Madison, Wisconsin 53706-1322, USA. Fax: 1 608 262 6143; Tel: 1 608 265 6288; E-mail: stahl@chem.wisc.edu

† Electronic Supplementary Information (ESI) available: Experimental and data-processing details, description of catalyst array preparation, tabulated activity data, Tafel plots, catalyst stability. See DOI: 10.1039/b000000x/

‡ Footnotes should appear here. These might include comments relevant to but not central to the matter under discussion, limited experimental and spectral data, and crystallographic data.

1 a) M. G. Walter, E. L. Warren, J. R. McKone, S. W. Boettchner, Q. Mi, E. A. Santori, N. S. Lewis, *Chem. Rev.*, 2010, **110**, 6446 - 6473; b) Á. Valdés, J. Brillet, M. Grätzel, H. Gudmundsdóttir, H. A. Hansen, H. Jónsson, P. Klüpfel, G.-J. Kroes, F. Le Formal, I. C. Man, R. S. Martins, J. K. Nørskov, J. Rossmeisl, K. Sivula, A. Vojvodic, M. Zäch, *Phys. Chem. Chem. Phys.*, 2012, **14**, 49 – 70; c) J. R. Swierk, T. E. Mallouk, *Chem. Soc. Rev.* 2013, **42**, 2357 – 2387.

2 a) H. Dau, C. Limberg, T. Reier, M. Risch, S. Roggan, P. Strasser, *ChemCatChem*, 2010, **2**, 724 - 761; b) V. Artero, M. Chavarot-Kerlidou, M. Fontecave, *Angew. Chem. Int. Ed.*, 2011, **50**,7238-7266; c) P. Du, R. Eisenberg, *Energy Environ. Sci.*, 2012, **5**, 6012 - 6021; d) A. Singh, L. Spiccia, *Coord. Chem. Rev.*, 2013, **257**, 2607 - 2622.

3 a) A. J. Esswein, M. J. McMurdo, P. N. Ross, A. T. Bell, T. D. Tilley, *J. Phys. Chem. C*, 2009, **113**, 15068-15072; b) F. Jiao, H. Frei *Angew. Chem. Int. Ed.*, 2009, **48**, 1841 - 1844; c) F. Jiao, H. Frei, *Chem. Commun.*, 2010, **46**, 2920 - 2922; d) B. S. Yeo, A. T. Bell, *J. Am. Chem. Soc.*, 2011, **133**, 5587 - 5593; e) H. S. Ahn, T. D. Tilley *Adv. Funct. Mater.*, 2012, **23**, 227 - 233.

4 a) M. W. Kanan, D. G. Nocera, *Science*, 2008, **321**, 1072-1075; b) Y. Surendranath, M. Dincă, D. G. Nocera, *J. Am. Chem. Soc.*, 2009, **131**, 2615-2620; c) Y. Gorlin, T. F. Jaramillo, *J. Am. Chem. Soc.*, 2010, **132**, 13612 - 13614; d) J. B. Gerken, E. C. Landis, R. J. Hamers, S. S. Stahl, *ChemSusChem*, 2010, **3**, 1176 - 1179; e) J. B. Gerken, J. G. McAlpin, J. Y. C. Chen, M. L. Rigsby, W. H. Casey, R. D. Britt, S. S. Stahl, *J. Am. Chem. Soc.*, 2011, **133**, 14431 - 14442; f) J. J. Stracke, R. G. Finke, *J. Am. Chem. Soc.*, 2011, **133**, 14872 - 14875.

5 B. V. Tilak, P. W. T. Lu, J. E. Colman, S. Srinivasan, in *Comprehensive Treatise of Electrochemistry*, Vol. 2, J. O'M. Bockris, B. E. Conway, E. Yeager, R. E. White, ed., Plenum, New York (1981), Chap. 1.

6 Co-based spinel catalysts have been recently reviewed in: M. Hamdani, R. N. Singh, P. Chartier, *Int. J. Electrochem. Sci.*, 2010, **5**, 556 - 577.

7 a) T. Otagawa, J. O'M. Bockris, *J. Electrochem. Soc.*, 1982, **129**, 2391 - 2392; b) J. Suntivich, K. J. May, H. A. Gasteiger, J. B. Goodenough, Y. Shao-Horn, *Science*, 2011, **334**, 1383 - 1385; c) K. J. May, C. E. Carlton, K. A. Stoerzinger, M. Risch, J. Suntivich, Y.-L. Lee, A. Grimaud, Y. Shao-Horn, *J. Phys. Chem. Lett.*, 2012, **3**, 3264 - 3270; d) A. Grimaud, C. E. Carlton, M. Risch, W. T. Hong, K. J. May, Y. Shao-Horn, *J. Phys. Chem. C*, 2013, **117**, 25926.

8 a) G. Młynarek, M. Paszkiewicz, A. Radniecka, *J. Appl Electrochem.*, 1984, **14**, 145 - 149; b) S. I. Córdoba, R. E. Carbonio, M. López Teijelo, V. A. Macagno, *Electrochim. Acta*, 1987, **32**, 749 - 755; c) D. A. Corrigan, *J. Electrochem. Soc.*, 1987, **134**, 377 - 384; d) E. L. Miller, R. E. Rocheleau, *J. Electrochem. Soc.*, 1997, **144**, 3072 - 3077; e) T.-C. Wen, H.-M. Kang, *Electrochim. Acta*, 1998, **43**, 1729 - 1745; f) M. I. Godinho, M. A. Catarino, M. I. da Silva Pereira, M. H. Mendonça, F. M. Costa, *Electrochim. Acta*, 2002, **47**, 4307 - 4314; g) R. N. Singh, J. P. Singh, H. Nguyen Cong, P. Chartier, *Int. J. Hydrogen Energy*, 2006, **31**, 1372 - 1378; h) M. Kumar, R. Awasthi, A. K. Pramanick, R. N. Singh, *Int. J. Hydrogen Energy*, 2011, **36**, 12698 - 12705; i) R. D. L. Smith, M. S. Prévot, R. D. Fagan, S. Trudel, C. P. Berlinguette, *J. Am. Chem. Soc.*, 2013, **135**. 11580-11586.

9 Y. J. Park, J. W. Ziller, A. S. Borovik, *J. Am. Chem. Soc.*, 2011, **133**, 9258 - 9261.

10 We admit to hedging our bets with some Lewis acids that may also be redox active at relevant potentials, such as, Cr, Ce, and Fe.

11 a) K. N. Ferreira, T. M. Iverson, K. Maghlaoui, J. Barber, S. Iwata, *Science* 2004, **303**, 1831 - 1838; b) J. Yano, J. Kern, Y. Pushkar, K. Sauer, P. Glatzel, U. Bergmann, J. Messinger, A. Zouni, V. K. Yachandra, *Phil. Trans. R. Soc. B*, 2008, **363**, 1139 - 1147; c) Y. Umena, K. Kawakami, J.-R. Shen, N. Kamiya, *Nature*, 2011, **473**, 55 - 60; d) I. Zaharieva, M. M. Najafpour, M. Wiechen, M. Haumann, P. Kurz, H. Dau, *Energy Environ. Sci.*, 2011, **4**, 2400 - 2408; e) P. Kurz, M. Wiechen, *Nachr. Chem.*, 2012, **60**, 24 - 28.

12 a) J. S. Kanady, E. Y. Tsui, M. W. Day, T. Agapie, *Science*, 2011, **333**, 733 - 736; b) M. Wiechen, I. Zaharieva, H. Dau, P. Kurz, *Chem. Sci.*, 2012, **3**, 2330 - 2339; c) F. H. M. Koua, Y. Umena, K. Kawakami, J.-R. Shen, *Proc. Natl. Acad. Sci. USA*, 2013, **110**, 3889 - 3894.

13 J. B. Gerken, J. Y. C. Chen, R. C. Massé, A. B. Powell, S. S. Stahl, *Angew. Chem. Int. Ed.*, 2012, **51**, 6676-6680.

14 a) M. Woodhouse, G. S. Herman, B. A. Parkinson, *Chem. Mater.*, 2005, **17**, 4318 - 4324; b) M. Woodhouse, B. A. Parkinson *Chem. Soc. Rev.*, 2009, **38**, 197 - 210; c) J. He, B. A. Parkinson, *ACS Comb. Sci.*, 2011, **13**, 399 - 404. d) B. A. Parkinson *Energy Environ. Sci.*, 2010, **3**, 509 - 511; e) G. R. Winkler, J. R. Winkler, *Rev. Sci. Instrum.*, 2011, **82**, 114101; f) http://www.thesharkproject.org/

15 a) E. Reddington, A. Sapienza, B. Gurau, R. Viswanathan, S. Sarangapani, E. S. Smotkin, T. E. Mallouk, *Science*, 1998, **280**, 1735 - 1737; b) G. Chen, D. A. Delafuente, S. Sarangapani, T. E. Mallouk, *Catal. Today*, 2001, **67**, 341 - 355; c) D. Seley, K. Ayers, B. A. Parkinson, *ACS Comb. Sci.*, 2013, **15**, 82 - 89; d) C. Xiang, S. K. Suram, J. A. Haber, D. W. Guevarra, E. Soedarmadji, J. Jin, J. M. Gregoire, *ACS Comb. Sci.*, 2014, **16**, 46 - 52.

16 a) C. M. Sánchez-Sánchez, J. Rodríguez-López, A. J. Bard, *Anal. Chem.*, 2008, **80**, 3254 - 3260; b) J. E. Katz, T. R. Gingrich, E. A. Santori, N. S. Lewis, *Energy Environ. Sci.*, 2009, **2**, 103 - 112; c) J. M. Gregoire, C. Xiang, S. Mitrovic, X. Liu, M. Marcin, E. W. Cornell, J. Fan, J. Jin, *J. Electrochem. Soc.*, 2013, **160**, F337 - F342; d) J. A. Haber, C. Xiang, D. Guevarra, S. Jung, J. Jin, J. M. Gregoire, *ChemElectroChem*, 2013, DOI: 10.1002/celc.201300229; e) J. A.

Haber, Y. Cai, C. Xiang, S. Mitrovic, J. Jin, A. T. Bell, J. M. Gregoire, *Energy Environ. Soc.*, 2014, **7**, 682 - 688.
17 J. Y. C. Chen, J. T. Miller, J. B. Gerken, S. S. Stahl, *Energy Environ. Sci.*, 2014, **7**, 1382 - 1386.
18 a) R. J. Meier, S. Schreml, X.-d. Wang, M. Landthaler, P. Babilas, O. S. Wolfbeis *Angew. Chem Int. Ed..*, 2011, **50**, 10893-10896; b) M. Schäferling, *Angew. Chem. Int. Ed.*, 2012, **51**, 3532-3554.
19 See ESI† for Java code used in image processing (Listings S1 & S2).
20 Image processing was performed with ImageJ: M. D. Abràmoff, P. J. Magalhães, S. J. Ram, *Biophotonics International*, 2004, **11**, 36 - 42.
21 D. M. Robinson, Y. B. Go, M. Mui, G. Gardner, Z. Zhang, D. Mastrogiovanni, E. Garfunkel, J. Li, M. Greenblatt, G. C. Dismukes, *J. Am. Chem. Soc.*, 2013, **135**, 3494 – 3501.
22 a) L. Trotochaud, J. K, Ranney, K. N. Williams, S. W. Boettcher, *J. Am. Chem. Soc.*, 2012, **134**, 17253 - 17261; b) J. Landon, E. Demeter, N. İnoğlu, C. Keturakis, I. E. Wachs, R. Vasić, A. I. Frenkel, J. R. Kitchin, *ACS Catal.*, 2012, **2**, 1793 - 1801; c) M. Gong, Y. Li, H. Wang, Y. Liang, J. Z. Wu, J. Zhou, J. Wang, T. Regier, F. Wei, H. Dai, *J. Am. Chem. Soc.*, 2013, **135**, 8452 - 8455; d) M. W. Louie, A. T. Bell, *J. Am. Chem. Soc.*, 2013, **135**, 12329 - 12337.
23 M. Kosmulski, *Adv. Colloid Interface Sci.*, 2009, **152**, 14 - 25.
24 e.g., the comparison between NiFe2O4 and NiGa2O4 in: S. Greenwald, S. J. Pickart, F. H. Grannis *J. Chem. Phys.*, 1954, **22**, 1597 - 1600.
25 A rigorous protocol for benchmarking OER catalysts has been recently described: C. C. L. McCrory, S. Jung, J. C. Peters, and T. F. Jaramillo *J. Am. Chem. Soc.*, 2013, **135**, 16977 - 16987.